Steel and Composite Structures, *Vol. 30, No. 5* (*2019*) *405-416*
DOI: https://doi.org/10.12989/scs.2019.30.5.405

Compressive behavior of profiled double skin composite wall

Ying Qin*, Yong-Wei Li, Yu-Sen Su, Xu-Zhao Lan, Yuan-De Wu and Xiang-Yu Wang

Key Laboratory of Concrete and Prestressed Concrete Structures of Ministry of Education,
School of Civil Engineering, *Southeast University*, *Nanjing*, *China*

(*Received November 5, 2018, Revised January 29, 2019, Accepted February 18, 2019*)

Abstract. Profiled composite slab has been widely used in civil engineering due to its structural merits. The extension of this concept to the bearing wall forms the profiled composite wall, which consists of two external profiled steel plates and infill concrete. This paper investigates the structural behavior of this type of wall under axial compression. A series of compression tests on profiled composite walls consisting of varied types of profiled steel plate and edge confinement have been carried out. The test results are evaluated in terms of failure modes, load-axial displacement curves, strength index, ductility ratio, and load-strain response. It is found that the type of profiled steel plate has influence on the axial capacity and strength index, while edge confinement affects the failure mode and ductility. The test data are compared with the predictions by modern codes such as AISC 360, BS EN 1994-1-1, and CECS 159. It shows that BS EN 1994-1-1 and CECS 159 significantly overestimate the actual compressive capacity of profiled composite walls, while AISC 360 offers reasonable predictions. A method is then proposed, which takes into account the local buckling of profiled steel plates and the reduction in the concrete resistance due to profiling. The predictions show good correlation with the test results.

Keywords: axial load; composite wall; steel-concrete-steel; capacity; failure mode

1. Introduction

Cold-formed steel tubes have been increasingly popular in civil engineering (Qin *et al*. 2018a). They sometimes serve as the formwork for concrete, which forms the concrete-filled tube columns (Qin *et al*. 2015a). The infilled concrete provides strong support for tube column and prevents the tube from buckling inward (Qin *et al*. 2018b). Plenty of research has been performed on the topic such as seismic performance (Qin and Chen 2016), local buckling (Qin *et al*. 2018c), and analytical modelling (Qin *et al*. 2015b). Similarly, cold-formed profiled steel plates have been widely used as the permanent formwork for reinforce concrete slabs (Saggaff *et al*. 2015, Qin *et al*. 2017a). This type of composite slabs offers substantial merits over conventional concrete slabs in terms of increased strength and stiffness, good ductility, reduced slab thickness, and efficient construction. Therefore, extensive studies have been conducted on the structural behavior, such as fire resistance (Bednar *et al*. 2013), long-term deflection (Gholamhoseini *et al*. 2014), flexural performance (Fang *et al*. 2016), longitudinal shear behavior (Kataoka *et al*. 2017), and shrinkage development (Al-Deen 2018), of composite slabs.

In recent years, the concept of profiled composite slabs has been extended to the application of profiled composite walls, which uses profiled steel plates as external skins and fills concrete inside. Besides all mentioned advantages associated with profiled composite slabs, the profiled composite wall uses the ribs of steel plate and the concrete core to prevent the local buckling (Yousefi and Ghalehnovi 2018). The profiled interface also eliminates the need for fasteners like shear studs if the wall is served as shear wall. Furthermore, the profiled composite walls reduce the wall thickness and lead to more available space in the buildings. These walls may act as bearing walls and can be applied to nuclear power plants due to their unique materials.

Profiled composite walls were initially proposed and studied by Wright (1998) and Hossain (2000) under axial loading. A series of axial compressive tests of profiled composite wall specimens were performed and design formulas was presented. Mydin and Wang (2011) and Prabha *et al*. (2013) allowed the use of lightweight foamed concrete as the concrete core for the composite walls. Their research indicated this structural system had sufficient load bearing capacity to be applied in low-rise residential construction. Rafiei *et al*. (2013) used finite element models to simulate the performance of profiled composite walls under in-plane shear loading. Hilo *et al*. (2016) proposed the application of embedded cold-formed steel tubes (ECFS) to strengthen the profiled composite walls. Finite element models were developed to perform parametric studies to evaluate the effect of ECFS thickness, number of the ECFS, and ECFS shapes on the loading carrying performance of the wall.

From the literature review, it can be found that most of the studies were conducted on the shear behavior of profiled composite walls to allow the walls to be used as lateral load resisting components. There is a dearth of information on the axial behavior of the wall (Wright 1998, Hossain 2000), which is necessary for the wall to be used as bearing wall in

*Corresponding author, Ph.D., Associate Professor,
E-mail: qinying@seu.edu.cn

http://www.techno-press.org/?journal=scs&subpage=6 ISSN: 1229-9367 (Print), 1598-6233 (Online)

building and nuclear power plant.

The available research on compressive behavior were conducted on profiled composite walls with internal fasteners, but the study on composite walls without internal fasteners was limited. As will be seen from the results in this paper, the compressive capacity of walls without internal fasteners is slightly lower than that of those with fasteners. However, the former type of wall has its own advantages. There is no need to weld shear studs or other fasteners and thus, the fabrication is much easier. Furthermore, it is more convenient to deliver and erect it on site. Therefore, both cost and time can be significantly reduced. Considering the fact that the ribs of steel plate and the concrete core prevent the local buckling under lateral force, the wall without internal fasteners can be applied to structures subjected to small amount of gravity load and large shear load such as non-load-bearing walls, gravity seawalls, floating breakwater, and protective structures.

Meanwhile, variability in types of profiled steel plates has not been paid enough attention in previous research by Wright (1998) and Hossain (2000), which has great influence on the axial performance. Furthermore, most of studied walls had exposed side edges. However, good confinement to the side edges will significantly enhance the axial behavior of wall, as will be seen later from the research in this paper.

This research aims for addressing the shortcomings of previous research mentioned above and as well, providing more available data of axial load behavior of profiled composite walls. This is achieved by carrying out experimental investigations on three specimens subjected to axial compressive loading. It highlights the performance of profiled composite walls based on the use of different types of profiled steel plates and side edge confinement.

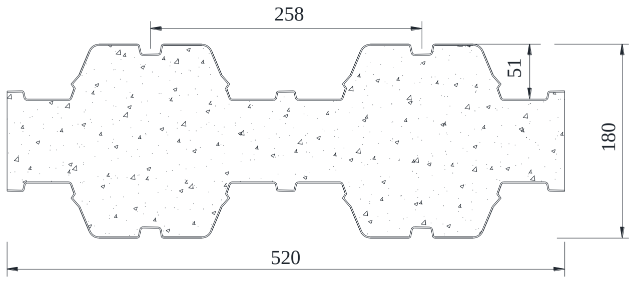

(a) Specimen PCW-1

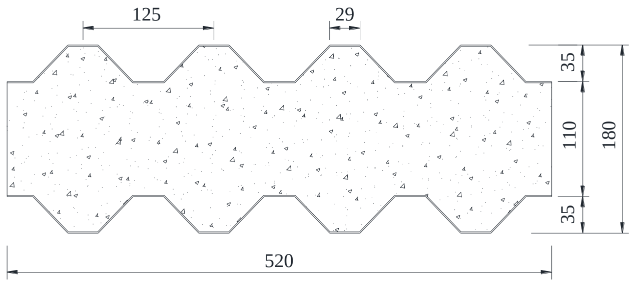

(b) Specimen PCW-2

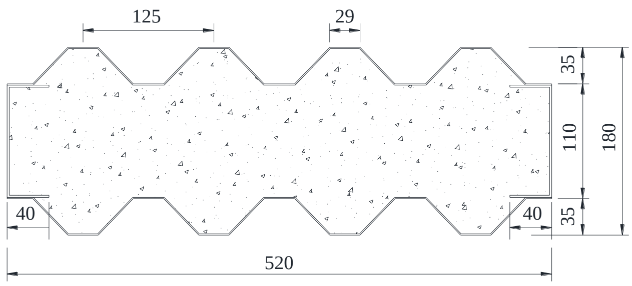

(c) Specimen PCW-3

Fig. 1 Geometry of test specimens

2. Experimental program

2.1 Geometrical description of specimens

Three sets of tests are conducted on profiled composite walls under axial compressive loading as shown in Table 1. The dimensions of the test specimens are 800 mm high × 520 mm wide × 180 mm thick. The variables in the tests are types of profiled steel plates and side edge confinement. The detailed geometry of the test specimens is shown in Fig. 1. The small height to thickness ratio means the failure of the specimens is expected to be controlled by cross-sectional capacity. It should be noted that in previous studies, threaded robs, tie bars or bolts were provided to act as the internal mechanical connector to lock the profied steel plate and concrete core together, which is necessary to achieve good composite action. However, there is no information on composite walls without connectors. The designed specimens in this research aim to filling this gap to evaluate the specimens without interface connectors, which will offer basic information on the axial behavior of profiled composite walls.

The difference between Specimens PCW-1 and PCW-2 is the type of profiled steel plate. YX51-253-760 and YX35-125-750, respectively, are used for the two specimens. This comparison aims to show the influence of shape of profiled steel plates on the axial behavior of the wall. Specimen PCW-3 uses the channel section with a thickness of 2 mm to act as the side confinement. This additional measurement is believed to be beneficial to the composite action between the profiled steel plates and the concrete core.

Table 1 Test specimens for compressive loading

Specimen No.	Wall dimension (height×width×thickness)	Type of profiled steel plate	Side edge confinement
	mm×mm×mm		
PCW-1	800×520×180	YX51-253-760	×
PCW-2	800×520×180	YX35-125-750	×
PCW-3	800×520×180	YX35-125-750	√

2.2 Casting

The profiled composite wall specimens were cast vertically with commercial concrete in the lab on the same day after the profiled steel plates had been assembled at the right location, in order to ensure that the concrete core in all specimens owns the identical compressive capacity. Three concrete cubes for material testing were cured at room temperature until the testing day. The cube tests gave an averaged cubic compressive strength of 24 MPa and the corresponding cylinder compressive strength was 18.24 MPa.

Three tensile coupons cut from the profiled steel plates of YX51-253-760 and YX35-125-750, respectively, were tested to determine the yield strength f_y, ultimate strength f_u, yield ratio f_y/f_u, modulus of elasticity E_s, and the elongation E_{lo}. The test results are provided in Table 2 and the stress versus strain curves are presented in Fig. 2.

Table 2 Material property

Type	Coupon No.	Thickness	f_y	f_u	f_y / f_u	E_s	E_{lo}
		mm	MPa	MPa		MPa	%
YX51 -253 -760	1	1.2	310.4	382.1	0.812	2.06×10^5	21.3
	2	1.2	303.2	382.1	0.794	2.05×10^5	21.1
	3	1.2	308.9	386.3	0.800	2.05×10^5	20.6
YX35 -125 -750	4	1.2	264.5	336.5	0.786	2.06×10^5	26.1
	5	1.2	260.9	331.5	0.787	1.92×10^5	27.1
	6	1.2	264.7	336.8	0.786	2.00×10^5	26.4

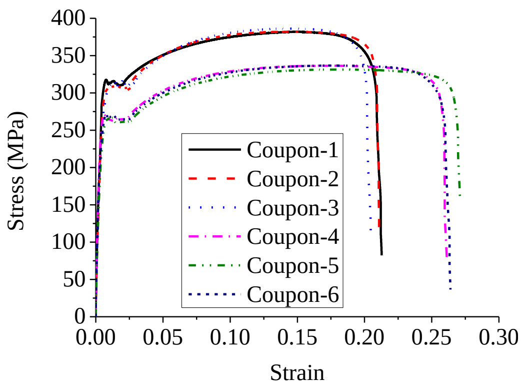

Fig. 2 Material property of profiled steel plate

Fig. 3 Test setup for profiled composite walls

2.3 Test setup and loading procedure

The test setup for compression test of profiled composite walls is shown in Fig. 3. A universal compression testing machine with a maximum capacity of 2000 kN was used to test the specimens. A quasi-static loading procedure was introduced in the load-controlled way. The load was applied at intervals of 50 kN to ensure the data recording and deformation observation.

3. Test results

3.1 Typical failure mode

Specimens PCW-1, PCW-2, and PCW-3 were all tested up to the failure. The failure modes of the tested specimens are given in Fig. 4. From the test results, it can be observed that the basic failure mode of specimens under compression is concrete splitting and crushing, followed by the separation between the profiled steel plates and the concrete and the subsequent local buckling of profiled steel plates. The failure characteristics of Specimens PCW-1 and PCW-2 initiated with the cracking sound emitted from the specimen when the load was about 10%-25% of the peak load. Cracks could be observed at the exposed sides of the concrete. After that, the profiled steel plates started to separate from the concrete core at the load level of about 80%-90% of the peak load. This largely reduced the composite action of the specimen. The developed splitting of the concrete resulted in the degradation of structural stiffness and the transfer of load to the profiled steel plates, which caused outwards local buckling. For Specimen PCW-3 under compression, the audible crack noise occurred when the load was close to the peak load. Simultaneously, local buckling of profiled steel plates was observed. After the test, two splitting cracks along both the width and depth of the wall could be found. The profiled steel plates were separated from the concrete along the width of the wall, while the profiled steel plates along the shorter sides were still in close contact with the concrete and provided certain confinement to the inner concrete.

3.2 Load-displacement curves

The load versus displacement responses of three specimens are plotted in Fig. 5. The axial displacement was obtained by recording the average value of three linear varying displacement transducers at the bottom of the test specimens. The trend of the structural behavior of three specimens is similar. The relationship between the compressive load and the axial shortening is almost linear at the early stage of loading. The curves steadily go up as the axial compression increases. The stiffness of the specimen then gradually decreases as the cracks in the concrete become severer and the local buckling of profiled steel plates progresses. After the ultimate strength is achieved, the load starts to decrease as the axial deformation

(a) Specimen PCW-1 (b) Specimen PCW-2 (c) Specimen PCW-3

Fig. 4 Failure modes of tested specimens

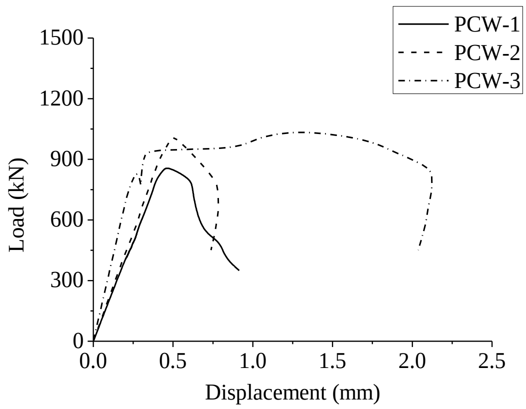

Fig. 5 Load-displacement curve

continues to grow.

The ultimate strength F_u and the corresponding axial displacement d_u of each specimen are listed in Table 3. It can be observed that the ultimate strength of Specimens PCW-2 and PCW-3 are close to each other, which means the edge confinement does not contribute to the load bearing capacity of the profiled composite walls and can be ignored in the calculation of capacity. In addition, the ultimate strength of Specimen PCW-1 is much smaller than that of the other two specimens. While the dimensions of three specimens are identical, the cross-sectional areas of concrete and steel in Specimen PCW-1 are 7697 mm^2 and 118 mm^2, respectively, smaller than those of the other two specimens. Those lost materials could approximately provide 146 kN bearing capacity if they are fully utilized. This value is close to the difference in capacity between Specimens PCW-1 and PCW-2 (or PCW-3).

It can also be observed that the axial displacement corresponding to the ultimate strength of Specimen PCW-3 is 173.4% and 152.8% greater than that of Specimens PCW-1 and PCW-2, respectively. As the axial load is approaching the ultimate strength, Specimen PCW-3 is able to sustain the capacity while develop considerable deformation. This indicates the edge confinement can provide more restraint to both profiled steel plates and the concrete core, which prohibits the crushing of concrete and postpones the local buckling of steel plates. Consequently, the good confinement to the side largely contributes to the deformation ability.

The initial stiffness of Specimens PCW-1 and PCW-2 is similar, while Specimen PCW-3 with edge confinement has noticeable higher stiffness. This indicates the initial stiffness of specimens is influenced by the overall dimension of the composite walls rather than the specific shape of profiled steel plates. Moreover, the edge confinement helps the two materials work together and delay the occurrence of either cracks or buckling and thus, enhance the stiffness of specimens. The calculated equation for the initial axial stiffness K_{theo} (Hao *et al*. 2017) is defined in Eq. (1).

$$K_{theo} = E_c A_c + E_s A_s \tag{1}$$

where E_c and E_s are the elastic modulus of concrete and steel, respectively, A_c and A_s are the cross-sectional area of concrete core and profiled steel plate, respectively. The calculated values of the three specimens are 2873 kN/mm, 3181 kN/mm, and 3126 kN/mm, respectively. It can be seen that the for Specimens PCW-1 and PCW-2, the theoretical values are 41.1% and 45.5%, respectively, higher than the

Table 3 Summary of test results

Specimen No.	F_u	d_u	$d_{0.85}$	μ	K	SI
	kN	mm	mm		kN/mm	
PCW-1	865	0.466	0.623	1.337	2036	0.561
PCW-2	1025	0.504	0.687	1.363	2187	0.666
PCW-3	1050	1.274	2.017	1.583	3411	0.637

tested ones, while for Specimen PCW-3, the predicted value is 8.4% lower than the tested one. This also shows that the composite action between the profiled steel plate and the concrete core can only be realized when edge confinement is appropriately provided.

3.3 Strength index (*SI*)

To evaluate the structural behavior of the profiled composite walls while exclude the influence of cross-sectional dimensions and steel ratio among specimens, strength index (SI) was introduced, which can be expressed as shown in Eq. (2).

$$SI = \frac{F_u}{0.85 f_c^{'} + f_y A_s} \tag{2}$$

where F_u is the peak load recorded in the tests, f'_c and f_y are the compressive strength of concrete and the yield strength of steel, respectively, A_c and A_s are the cross-sectional areas of concrete and steel, respectively.

According to Eq. (2), Table 3 lists the strength index *SI* of all specimens. The values of *SI* for three specimens are0.561, 0.666, and 0.637, respectively. It can be seen that the composite wall with YX35-125-750 profiled sheet works better than that with YX51-253-760 profiled sheet. This indicates that the structural capacity of specimens may benefit from more waves in the profiled steel plate. Furthermore, the specimen with edge confinement exhibits similar *SI* to the specimen without edge confinement, which means the edge confinement may not affect the capacity utilization of composite walls. It can also be observed that the cross-sectional capacities of all test specimens are not fully utilized. The yielding strength of the profiled steel plates may not be reached due to the local buckling of steel plates following the concrete crash. Additionally, the concrete core may not achieve its compressive strength due to the boundary conditions of the profile-shaped concrete is different from those of cylinder sample subjected to compression. Meanwhile, reduction may be considered for the profiled shape of concrete core.

3.4 Ductility ratio (*μ*)

Ductility is defined as the ability of the specimens to undergo large plastic deformation without obvious loss of strength (Qin *et al*. 2016~~b~~, 2019). It is an important parameter in structural design. The assessment of ductility for profiled composite walls can be carried out by calculating ductility ratio *m*, which is defined as the ratio of the axial displacement corresponding to 85% ultimate strength during the descending stage $d_{85\%}$ to the axial displacement corresponding to the ultimate strength d_u, as shown in Eq. (3). Table 2 lists the ductility ratio. It is found that the specimen with edge confinement, i.e., Specimens PCW-3, has higher ductility ratio, since both the crushing of concrete and the local buckling of profiled steel plates are delayed by using side plates. Moreover, the ductility ratio slightly increases in Specimen PCW-2 comparing to Specimen PCW-1, mainly because the YX35-125-750 type provides better confinement to concrete core than the YX51-253-760 does.

$$\mu = \frac{d_{85\%}}{d_u} \tag{3}$$

3.5 Load-strain curves

Each specimen was instrumented with strain gauges, as sketched in Fig. 6. On each steel face, three rows of strain gauges were placed along the direction of wall height at equal spacing (i.e., 100 mm, 400 mm, and 700 mm from the bottom) to capture the strain distribution along the specimen. One additional row of strain gauges was placed 250 mm from the bottom along the transverse to monitor the lateral strain development.

Figs. 7-9 show the load-strain curves for steel surface of each specimen. As can be seen, the strains at the same locations on two opposite sides are almost symmetrical, which indicates the specimens are under axial compression. The axial strains at the same row show similar trends as the load increases. The strain values grow linearly at the beginning of loading until the profiled steel plate starts to buckle. After that, the strains at the same row behave in slightly different ways. The strains begin to develop quickly at the descending stage of loading. At this stage, the specimens could fully deform to absorb more energy while sustain considerable loading-carrying ability. In addition, the lateral strains are normally quite small and behave in a linear way during the early loading stage. The strains become significant when the local buckling of profiled steel plate occurs. The values of lateral strains are obviously less than those of axial strains under the same level of loadings. This is expected as the axial shortening is the main deformation for the walls under compression.

It can found that most of the strain values corresponding to the ultimate strength of the test specimens are significantly less than the yielding value, which means the profiled steel plate does not reach its yielding strength when approaching the peak load. This is because the steel plate suffers from local buckling after the cracks occur in the concrete core. Therefore, buckling strength rather than yielding strength should be used to calculate the compressive capacity of composite wall. Furthermore, the comparison among three specimens also shows that more strains develop in Specimen PCW-3 than in the other two specimens for strain gauges at the same levels. This indicates that due to the better confinement in Specimen PCW-3, the resistance of steel plate can be more utilized and the overall structural capacity can thus increase.

It is interesting that for the strain gauges in the same row, more strains occur at the edge of the profiled steel plate than in the middle. This is because the infill concrete provides better restraint to the steel plate and prohibits the local buckling from occurring there, while the confinement to the steel plate at the edge is relative weak, which causes the strains develop more quickly.

Meanwhile, it can be found from Fig. 7 that the strains in the same column of Specimen PCW-1 gradually decrease as the distance from the loading surface, which means that the axial load applied on steel plate has been partially

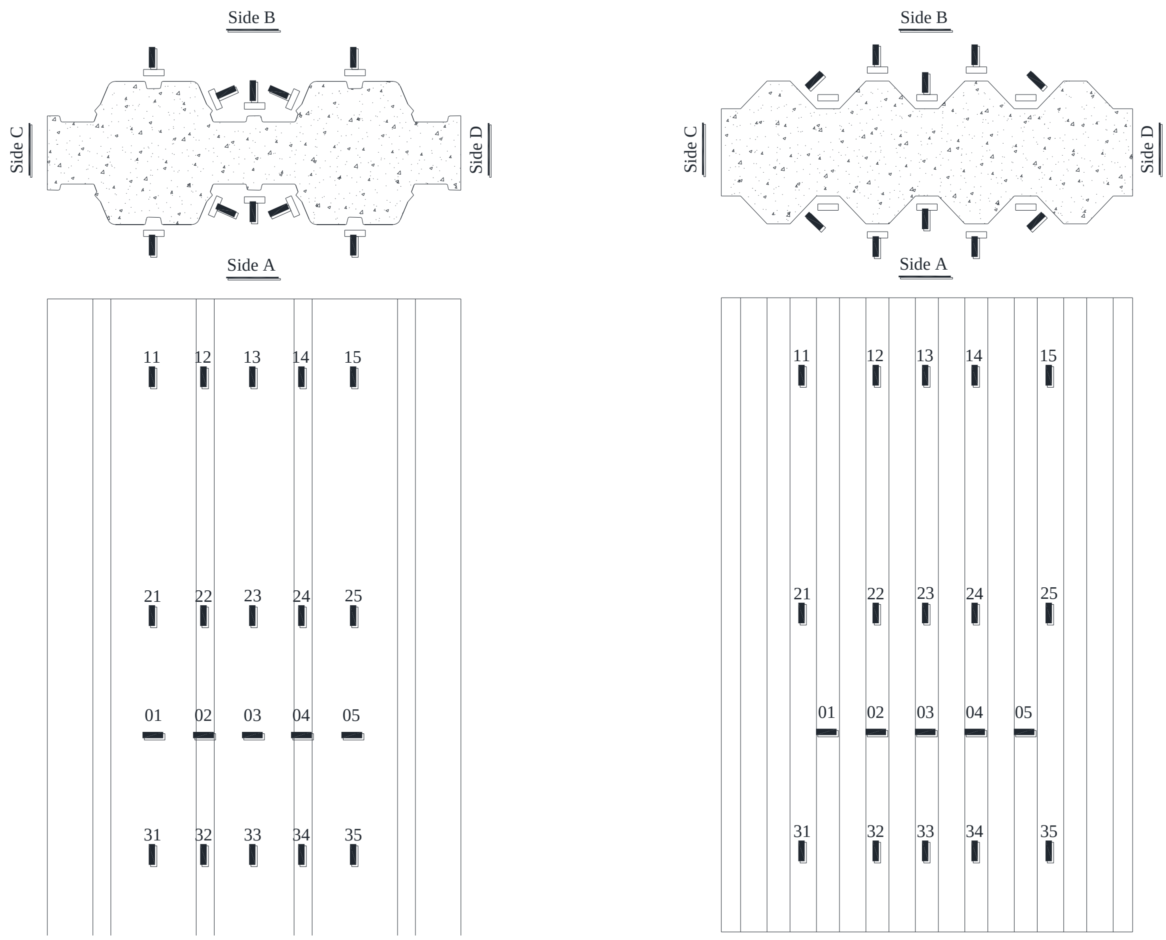

(a) Specimen PCW-1t (b) Specimens PCW-2 and PCW-3

Fig. 6 Arrangement of strain gauges

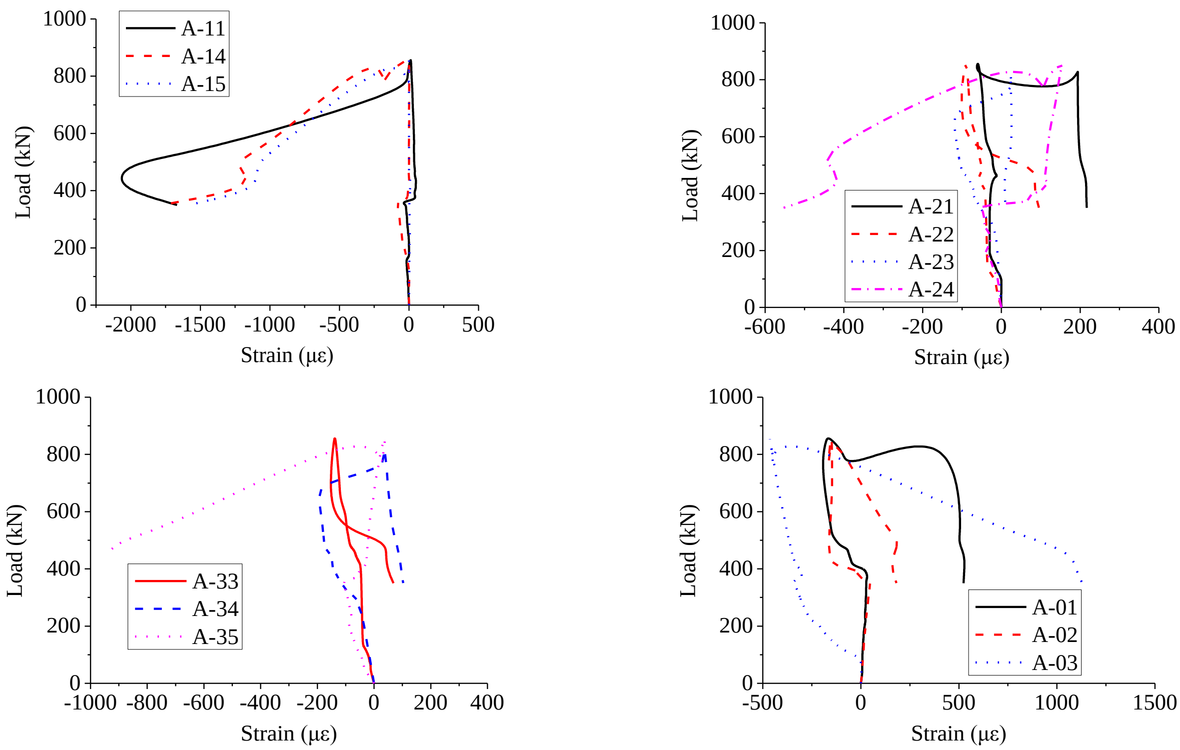

Fig. 7 Load-strain curve for Specimen PCW-1

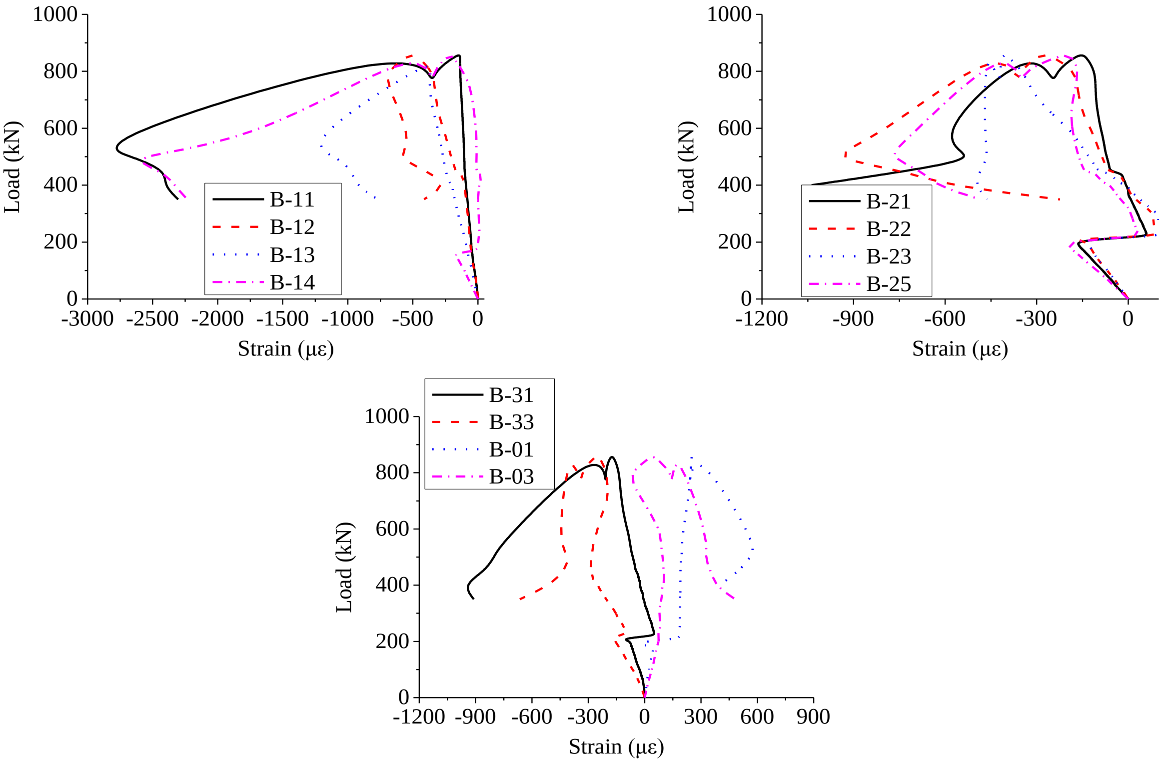

Fig. 7 Continued

transferred to the concrete core. This may be cuased by the early buckling of steel plate in Specimen PCW-1. The buckled steel plate is not able to sustain the axial compression and force the load burdened by the concrete. In contrast, Figs. 8-9 show that the strains in the same column of Specimens PCW-2 and PCW-3 almost uniformly distributed along the height of the walls. This means composite action is better achieved in these two specimens. Type YX35-125-750 with more profiled waves offers better restraint to thin steel plate that type YX51-253-760.

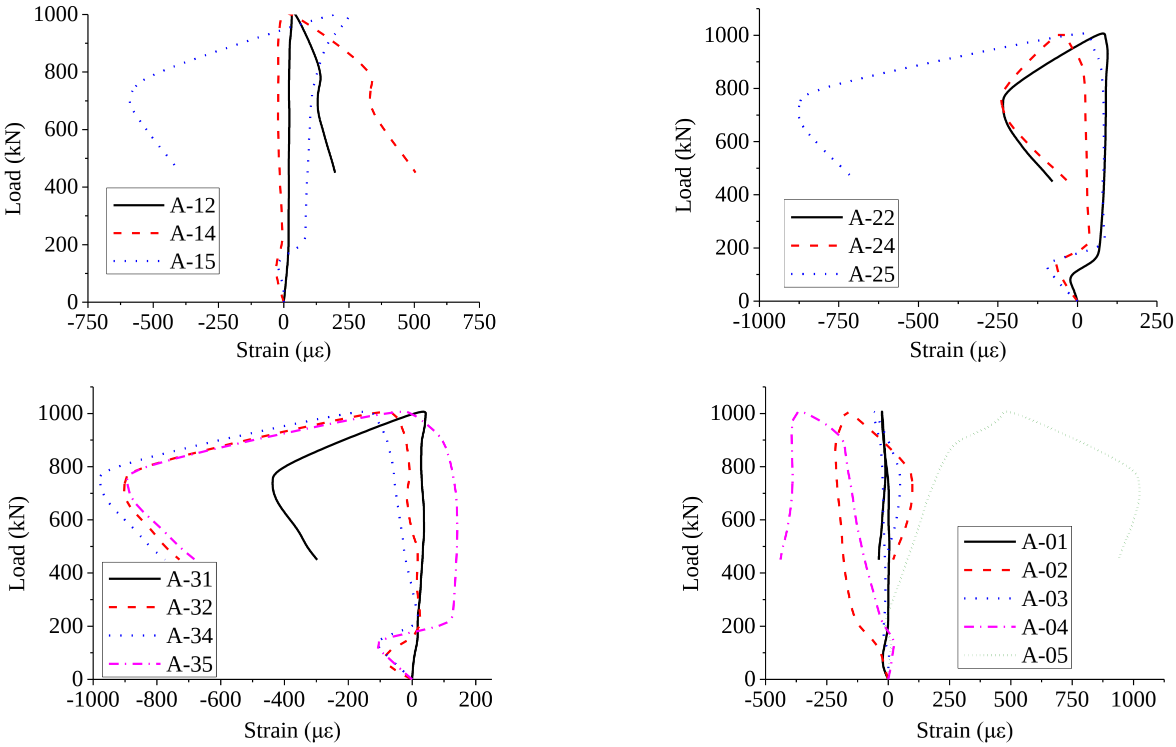

Fig. 8 Load-strain curve for Specimen PCW-2

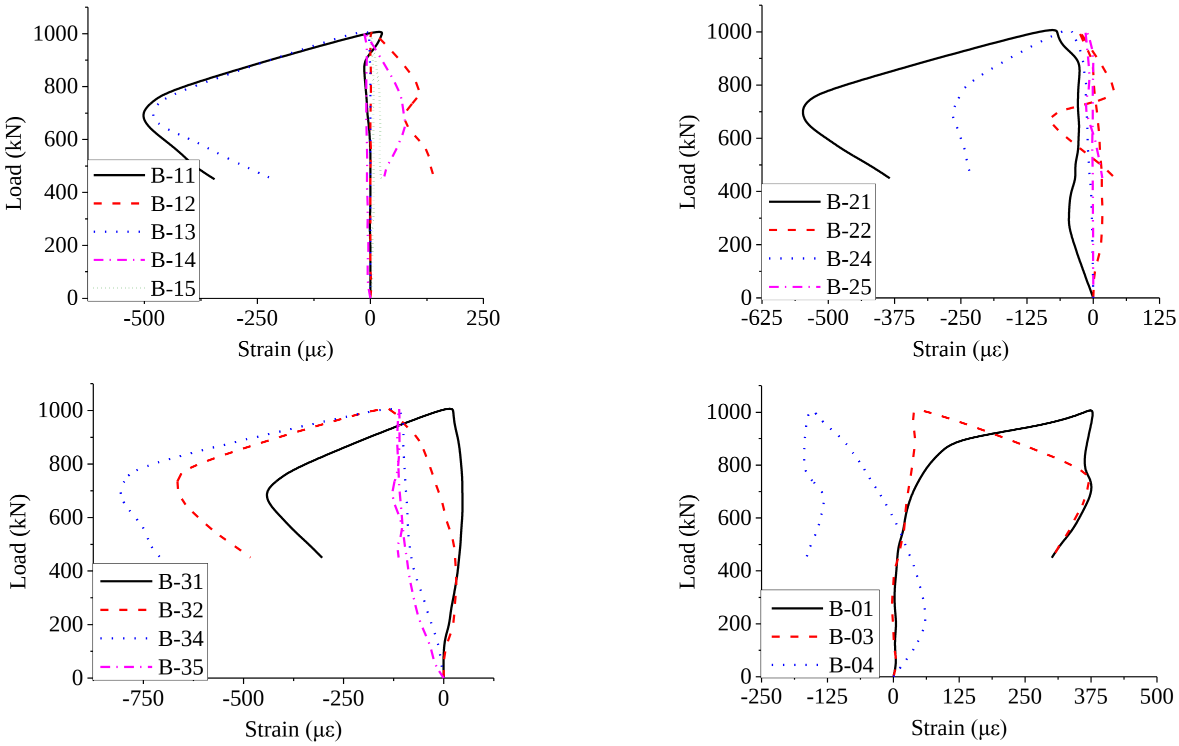

Fig. 8 Continued

When the profiled composite walls with thin steel plate are under axial compressive loading, local buckling occurs on steel plate. However, due to the restraint offered by the concrete infill, the steel plates only buckle outward with half-waves. When local buckling starts to develop on steel plate, the strain abruptly changes at the location. In this way, the possible buckling load could be determined. According to load-strain response shown in Fig. 7, for Specimen PCW-1, the buckling occurs on Side A at the loading level of 350 kN, while on side B the corresponding load is 180 kN. Similarly, as can be seen from Fig. 8, for Specimen PCW-2, the buckling load on Side A is 100 kN

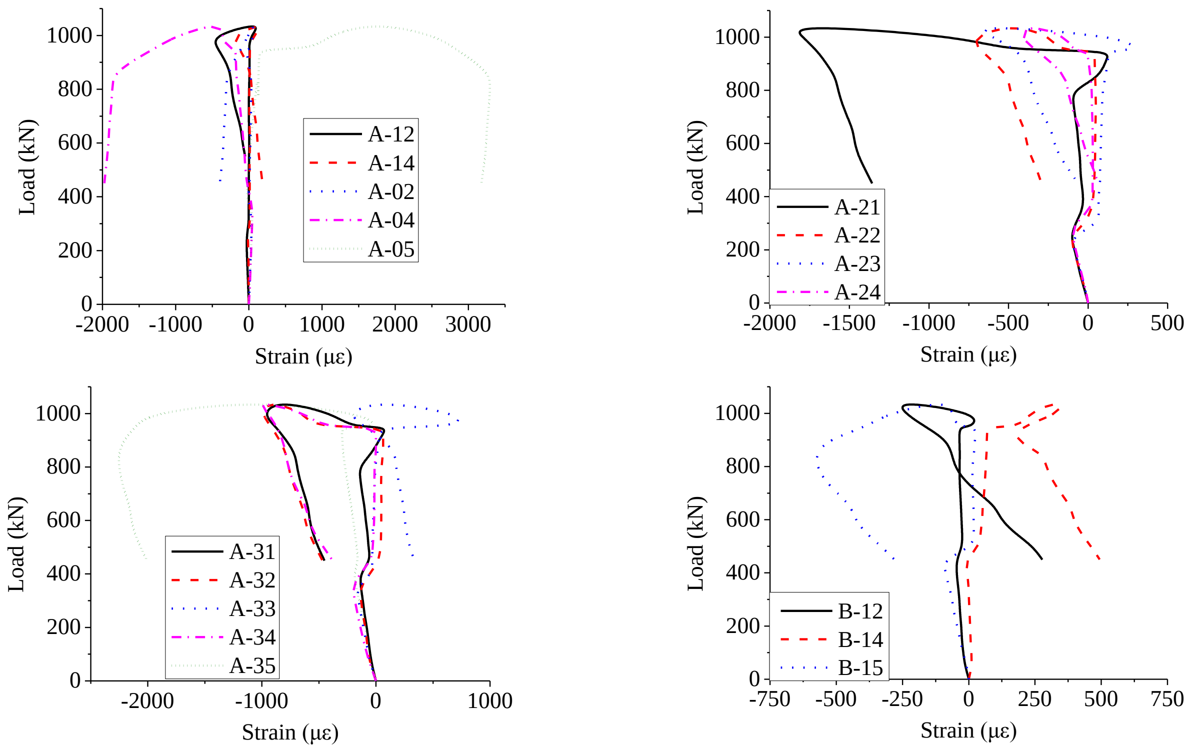

Fig. 9 Load-strain curve for Specimen PCW-3

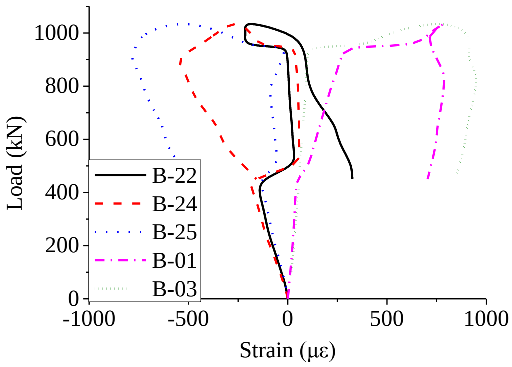

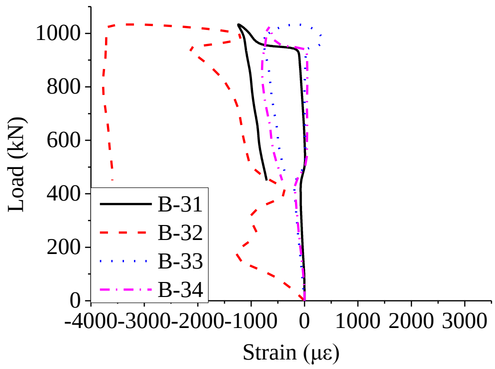

Fig. 9 Continued

and that on Side B is 130 kN. Based on the observation in Fig. 9, the buckling load for Specimen PCW-3 on Side A is 260 kN and that on Side B is 420 kN. The comparison between Specimens PCW-2 and PCW-3 shows that good edge confinement obviously prevents the local buckling of steel plate and thus, largely increases the buckling load.

4. Discussion on code design

4.1 AISC 360-16

Section I2 of AISC 360-16 (2016) provides the specifications for the designed compressive strength of composite members composed of rolled or built-up structural steel shapes and structural concrete acting together. Filled composite sections are classified as compact, noncompact or slender depending on the structural section slenderness. A profiled composite wall can be considered as slender section. It can neither develop yielding of the steel sheet in the longitudinal direction, nor confine the concrete after it reaches $0.70f'_c$ compressive stress in the concrete and starts undergoing inelastic strains and significant volumetric dilation pushing against the steel sheet. Therefore, profiled composite walls are limited to developing the critical buckling stress, F_{cr}, of the steel sheet and $0.70f'_c$ of the concrete infill. Effective stress-strain method provides guidance for calculating the cross-section strength of profiled composite walls, as shown in Eq. (4).

$$F_{u,AISC} = F_{cr} A_s + 0.7 f_c' A_c \tag{4}$$

where A_c = area of concrete, A_s = cross-sectional area of steel section, and other parameters can refer to AISC 360 for detailed information.

It should be noted that the code does not provide the calculation method of F_{cr} for profiled section. For rectangular filled sections F_{cr} could be determined by Eq. (5), while for round filled sections F_{cr} could be determined by Eq. (6).

$$F_{cr} = \frac{9E_s}{(b/t)^2} \tag{5}$$

$$F_{cr} = \frac{0.72F_y}{\left[\left(D/_t\right)\left(F_y/_{E_s}\right)\right]^{0.2}} \tag{6}$$

4.2 BS EN 1994-1-1

Clause 6.7 of BS EN 1994-1-1 (2004) gives the design approach of composite compression members with concrete encased sections, partially encased sections and concrete filled rectangular and circular tubes. The plastic resistance to compression $F_{u,Euro}$ of a composite cross-section is calculated by adding the plastic resistance of its components with reduction factor for possible additional compressive bending stresses created during slight eccentric loading or initial imperfections and reduced strength of concrete, as shown in Eq. (7).

$$F_{u,Euro} = f_y A_s + 0.85 f_c' A_c \tag{7}$$

4.3 CECS 159

Section 6 of CECS 159 (2004) offers the calculation formulas for the axially-loaded composite members, as given by Eq. (8). It assumes that the axial compressive capacity of composite walls is the superposition of the full contribution from both steel and concrete.

$$F_{u,CECS} = f_y A_s + f_c' A_c \tag{8}$$

4.4 Proposed method

Experimental investigations reveal that the axial load capacity of the profiled composite wall is affected by the local buckling of profiled steel plates and the reduced effective area of concrete cross-sectional area due to profiling. The research by Wright (1998) also indicated that the load bearing capacity of profiled concrete core was reduced when compared to solid concrete core. However, the influences of these two factors are not considered in equations incorporated in modern codes.

For profiled thin-walled structures, effective width is used to account for local buckling in current design method. Therefore, the ultimate strength of the profiled steel plate is approximately given by multiplying the yield stress f_y by the effective area $b_{eff}t$. In this research, the method proposed by Mydin and Wang (2011) was used to calculate the reduced strength of profiled steel plate. For profiled concrete core, the ribs of the profile do not present a solid mass of concrete and the extra bending stress due to possible loading eccentricity or material non-uniformity should be carried by the rib concrete (Mydin and Wang 2011). This reduces the load bearing capacity of the rib to carry the applied axial force. Instead of using a reduction factor as a function of the ratio of area of profile voids on one face to area of concrete as applied by Mydin and Wang (2011), in this paper, it suggests to simply exclude the profiled cross section when calculating the contribution from concrete. Therefore, the axial capacity $F_{u,p}$ of the profiled composite wall is assumed to be the sum of the reduced strength of profiled steel plates and the reduced concrete capacity, as shown in Eq. (9).

$$F_{u,p} = b_{eff}\,t f_y + 0.85 f_c^{'} A_{ceff} \tag{9}$$

Where A_{ceff} is the effective concrete area excluding the profiled cross section, as shown in Fig. 10. b_{eff} is the effective width of steel plate.

The research by Winter (1947) and Liang and Uy (2000) were adopted by Mydin and Wang (2011) to determine the effective width of steel plate. It was given below for the completeness of the paper.

According to the study by Winter (1947), the effective width b_{eff} of a profiled plate of the original width b can be calculated by Eq. (10).

$$\frac{b_{eff}}{b} = \sqrt{\left(\frac{\sigma_{cr}}{f_y}\right)\left[1 - 0.22\sqrt{\left(\frac{\sigma_{cr}}{f_y}\right)}\right]} \tag{10}$$

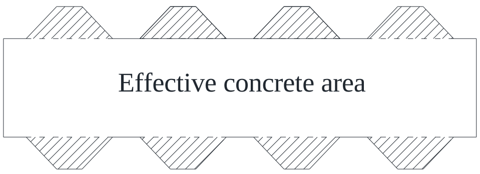

Fig. 10 Effective concrete area

Liang and Uy (2000) used the finite element method to study the post-local buckling behavior of steel plates in concrete-filled tube columns. They developed a novel method to evaluate the post-local buckling strength of steel plates with imperfections. Two effective width formulas were proposed for the design of steel plates restrained by concrete and were used to predict the ultimate strength of short concrete-filled tube columns, as given by Eqs. (11)-(12).

$$\frac{b_{eff}}{b} = 0.675\left(\frac{\sigma_{cr}}{f_y}\right)^{1/3} \quad \text{for} \quad \sigma_{cr} \le f_y \tag{11}$$

$$\frac{b_{eff}}{b} = 0.915\left(\frac{\sigma_{cr}}{\sigma_{cr} + f_y}\right)^{1/3} \quad \text{for} \quad \sigma_{cr} > f_y \tag{12}$$

where s_{cr} is the critical local buckling stress and can be expressed by Eq. (13).

$$\sigma_{cr} = \frac{k\pi^2 E_s}{12(1-\nu^2)(b/t)^2} \le f_y \tag{13}$$

where n is the Poison's ratio of steel and can be taken as 0.3, k is the elastic buckling coefficient, and b is the effective width of steel plate. For YX35-125-750 with only one wave in each profiled shape, b is taken as the wave length, while for YX51-253-760 with two small waves in each profiled shape, b is taken as half of the wave length.

The critical buckling coefficient k of the steel plate largely relies on the boundary conditions. Therefore, the critical buckling coefficient is a function of the boundary condition along the edges. Several researchers have proposed k values for various boundary conditions. Uy and Bradford (1996) suggested the k value of 0.8 for boundary consition of simply supported loaded edges and free unloaded edges (SF), while Qin *et al*. (2017b) proposed the k value of 5.467 for clamped loaded edges and simply-supported unloaded edges (CS).

Table 4 compares the compressive capacity obtained by the modern codes, the proposed method with k = 0.8 and k = 5.467, and the test results. Fig. 11 plots the test results and predictions. It is found that the predictions by BS EN 1994-1-1 and CECS 159 all significantly overestimate the axial compressive capacity of the test composite walls. The

Table 4 Comparison between the codes and the test results

Specimen No.	F_{AISC} (kN)	F_{Euro} (kN)	F_{CECS} (kN)	Winter (1947)		Liang and Uy (2000)		$\frac{F_u}{F_{AISC}}$	$\frac{F_u}{F_{Euro}}$	$\frac{F_u}{F_{CECS}}$	Winter (1947)		Liang and Uy (2000)	
				$F_{pk=0.8}$ (kN)	$F_{p,k=5.467}$	$F_{p,k=0.8}$	$F_{p,k=5.467}$				$\frac{F_u}{F_{p,k=0.8}}$	$\frac{F_u}{F_{p,k=5.467}}$	$\frac{F_u}{F_{p,k=0.8}}$	$\frac{F_u}{F_{p,k=5.467}}$
PCW-1	854	1542	1721	851	1010	867	972	1.013	0.561	0.503	1.016	0.856	0.998	0.890
PCW-2	949	1539	1740	985	1131	997	1095	1.080	0.666	0.589	1.041	0.906	1.028	0.936
PCW-3	948	1648	1847	978	1124	990	1088	1.108	0.637	0.568	1.074	0.934	1.061	0.965
Average								1.067	0.621	0.553	1.043	0.899	1.029	0.93
Standard deviation								0.040	0.044	0.037	0.023	0.032	0.026	0.031

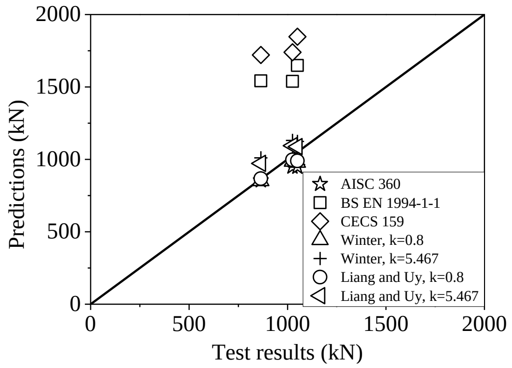

Fig. 11 Comparison between codes and test results

average ratios of the test results to the predictions by these two modern codes are 0.621 and 0.553, respectively. This is because the profiled steel plate does not reach its yielding strength when the peak load is achieved. Local buckling occurs early following the concrete crushing during the axial loading. Furthermore, the concrete core with profiled shape cannot fully utilize its compressive strength, and reduction due to profiling is not taken into account in these two modern codes. In contrast, AISC 360 provides reasonable predictions with the mean value of 1.067 and the standard deviation of 0.040. This is because both the strength of steel plate and concrete have been reduced in AISC 360.

Meanwhile, The effective width methods by Winter (1947) and Liang and Uy (2000) offer similar results. Moreover, the proposed method with k = 0.8 offers the best predictions. The ratio of the tested values to the predicted ones based on Winter (1947) range from 1.016 to 1.074 with a mean of 1.043 and a standard deviation of 0.023, while the ratio based on Liang and Uy (2000) range from 0.998 to 1.061 with a mean of 1.029 and a standard deviation of 0.026. It indicates that the boundary condition for steel sheet in composit wall is more likely to be simply supported along loaded edges and free along the unloaded edges. Referring to the study by Wright (1998), the composite walls with hook connectors could exhibit satisfactory load-carrying capacity, which is almost the summation of the capacity by steel and concrete. This indirectly verifies the necessity to arrange internal connectors to achieve better composite action between profiled steel plate and concrete core.

5. Conclusions

This paper investigates the axial loading behavior of profiled composite walls. Axial compressive tests are conducted, and the considered variables are the types of profiled steel plate and the edge confinement. The test results are analyzed in terms of failure mode, load-displacement response, strength index, ductility ratio, and load-strain relation. The method to calculate the axial compressive capacity of profiled composite walls has been proposed. The following conclusions are drawn from the study.

(1) The failure of profiled composite walls under compression is caused by concrete crushing, followed by the separation between steel and concrete and the subsequent local buckling of steel plates. The cross-sectional resistance of the wall is not fully utilized.
(2) The type of profiled steel plate has influence on the compressive capacity and strength index due to the differences in cross-sectional area and geometry. The edge confinement is beneficial to the wall ductility, since it can delay the crushing of concrete and prevent the steel plate from early buckling. Moreover, good confinement is essential for the composite action between steel and concrete to be realized. However, the effect of edge confinement on the compressive capacity and the strength index is negligible.
(3) The modern codes, i.e., BS EN 1994-1-1 and CECS 159, both provide over estimation of the test results, while AISC 360 offers reasonable predictions. This is due to the fact that the local buckling of steel plate and the reduction in profiled concrete core are not taken into account into the design equations in former two codes. The proposed method for prediction of compressive capacity in this paper is based on the reduced contribution from both profiled steel plate and concrete core. The predicted values are compared with test data and are found to be adequate.

Acknowledgments

This work is sponsored by the Natural Science Foundation of Jiangsu Province (Grant No. BK20170685), the National Key Research and Development Program of China (Grant No. 2017YFC0703802), and the Fundamental Research Funds for the Central Universities. The authors would like to thank the Jiangsu Xinlantian Steel Structure Co. Ltd. for the supply of test specimens.

References

AISC 360-16 (2016), Specification for structural steel buildings; American Institute of Steel Construction, Chicago, IL, USA.

Al-Deen, S. (2018), “Hydro-mechanical analysis of non-uniform shrinkage development and its effects on steel-concrete composite slabs”, *Steel Compos. Struct., Int. J.*, **26**(3), 303-314.

Bednar, J., Wald, F., Vodicka, J. and Kohoutkova, A. (2013), “Experiments on membrane action of composite floors with steel fibre reinforced concrete slab exposed to fire”, *Fire Safety J.*, **59**, 111-121.

BS EN 1994-1-1 (2004), Eurocode 4: Design of composite steel and concrete structures-Part 1-1: General rules and rules for buildings; British Standards Institution, London, UK.

CECS 159 (2004), Technical specification for structures with concrete-filled rectangular steel tube members; China Association for Engineering Construction Standardization, Beijing, China.

Fang, H., Xu, X., Liu, W.Q., Qi, Y.J., Bai, Y., Zhang, B. and Hui, D. (2016), “Flexural behavior of composite concrete slabs

reinforced by FRP grid facesheets", *Compos. Part B-Eng.*, **92**, 46-62.
Gholamhoseini, A., Gilbert, R.I., Bradford, M. and Chang, Z.T. (2014), "Time-Dependent Deflection of Composite Concrete Slahs", *ACI Struct., J.*, **111**(4), 765-775.
Hao, T.Y., Cao, W.L., Qiao, Q.Y., Liu, Y. and Zheng, W.B. (2017), "Structural performance of composite shear walls under compression", *Appl. Sci.-Basel*, **7**(2), 162.
Hilo, S.J., Badaruzzaman, W.H.W., Osman, S.A. and Al-Zand, A.W. (2016), "Structural behavior of composite wall systems strengthened with embedded cold-formed steel tube", *Thin Wall Struct.*, **98**, 607-616.
Hossain, K.M.A. (2000), "Axial load behaviour of pierced profied composite walls", *IPENZ Transaction*, **27**(1), 1-7.
Kataoka, M.N., Friedrich, J.T. and El Debs, A.L.H.C. (2017), "Experimental investigation of longitudinal shear behavior for composite floor slab", *Steel Compos. Struct., Int. J.*, **23**(3), 351-362.
Liang, Q.Q. and Uy, B. (2000), "Theoretical study on the post-local buckling of steel plates in concrete-filled box columns", *Comput. Struct.*, **75**, 479-490.
Mydin, M.A.O. and Wang, Y.C. (2011), "Structural performance of lightweight steel-foamed concrete-steel composite walling system under compression", *Thin Wall Struct.*, **49**, 66-76.
Prabha, P., Marimuthu, V., Saravanan, M., Palani, G.S., Lakshmanan, N. and Senthil, R. (2013), "Effect of confinement on steel-concrete composite light-weight load-bearing wall panels under compression", *J. Constr. Steel Res.*, **81**, 11-19.
Qin, Y. and Chen, Z.H. (2016), "Research on cold-formed steel connections: A state-of-the-art review", *Steel Compos. Struct., Int. J.*, **20**(1), 21-41.
Qin, Y., Chen, Z.H. and Rong, B. (2015a), "Component-based mechanical models for concrete-filled RHS connections with diaphragms under bending moment", *Adv. Struct. Eng.*, **18**(8), 1241-1255.
Qin, Y., Chen, Z.H. and Rong, B. (2015b), "Modeling of CFRT through-diaphragm connections with H-beams subjected to axial load", *J. Contr. Steel Res.*, **114**, 146-156.
Qin, Y., Chen, Z.H., Bai, J.J. and Li, Z.L. (2016), "Test of extended thick-walled through-diaphragm connection to thick-walled CFT column", *Steel Compos. Struct., Int. J.*, **20**(1), 1-20.
Qin, Y., Shu, G.P., Fan, S.G., Lu, J.Y., Cao, S. and Han, J.H. (2017a), "Strength of double skin steel-concrete composite walls", *Int. J. Steel Struct.*, **17**(2), 535-541.
Qin, Y., Lu, J.Y. and Cao, S. (2017b), "Theoretical study on local buckling of steel plate in concrete filled tube column under axial compression", *ISIJ Int.*, **57**(9), 1645-1651.
Qin, Y., Zhang, J.C., Shi, P., Chen, Y.F., Xu, Y.H. and Shi, Z.Z. (2018a), "Behavior of improved through-diaphragm connection to square tubular column under tensile loading", *Struct. Eng. Mech., Int. J.*, **68**(4), 475-483.
Qin, Y., Shu, G.P., Du, E.F. and Lu, R.H. (2018b), "Buckling analysis of elastically-restrained steel plates under eccentric compression", *Steel Compos. Struct., Int. J.*, **29**(3), 379-389.
Qin, Y., Du. E.F., Li, Y.W. and Zhang, J.C. (2018c), "Local buckling of steel plates in composite structures under combined bending and compression", *ISIJ Int.*, **58**(11), 2133-2141.
Qin, Y., Shu, G.P., Zhou, X.L., Han, J.H. and He, Y.F. (2019), "Height-thickness ratio on axial behavior of composite wall with truss connector", *Steel Compos. Struct., Int. J.*, **30**(4), 315-325. DOI: https://doi.org/10.12989/scs.2019.30.4.315
Rafiei, S., Hossain, K.M.A., Lachemi, M., Behdinan, K. and Anwar, M.S. (2013), "Finite element modeling of double skin profiled composite shear wall system under in-plane loadings", *Eng. Struct.*, **56**, 46-57.
Saggaff, A., Tahir, M.M., Sulaiman, A., Ngian, S.P. and Mirza, J. (2015), "Standardization of composite connections for trapezoid web profiled steel sections", *Struct. Eng. Mech., Int. J.*, **55**(4), 765-784.
Uy, B. and Bradford, M.A. (1996), "Elastic local buckling of steel plates in composite steel-concrete members", *Eng. Struct.*, **18**, 193-200.
Winter, G. (1947), "Strength of thin steel compression flanges", *Trans ASCE*, **112**, 527-554.
Wright, H.D. (1998), "The axial load behaviour of composite walling", *J. Constr. Steel Res.*, **45**(3), 353-375.
Yousefi, M. and Ghalehnovi, M. (2018), "Finite element model for interlayer behavior of double skin steel-concrete-steel sandwich structure with corrugated-strip shear connectors", *Steel Compos. Struct., Int. J.*, **27**(1), 123-133.

CC